Supplementary Information: Universal, high-fidelity quantum gates based on superadiabatic, geometric phases on a solid-state spin-qubit at room temperature

Felix Kleißler[1,*], Andrii Lazariev[1], and Silvia Arroyo-Camejo[1,]**

[1]Max Planck Institute for Biophysical Chemistry, Department of NanoBiophotonics, Am Faßberg 11, 37077 Göttingen, Germany
[*]fkleiss@mpibpc.mpg.de
[**]sarroyo@mpibpc.mpg.de

1 Accelerated driving field frames

The superadiabatic geometric quantum gate is defined on the two-dimensional Hilbert space $\mathscr{H}^2$ and is driven by a time-dependent field. Consequentially, the Hamiltonian in the laboratory frame $H_L(t)$ follows as the one of a two-level system with energy spacing $\hbar\omega_0$ and a driving field of angular frequency $\omega_D(t)$, phase φ and amplitude $\Omega_{\mathrm{R}}(t)$:

$$\begin{aligned} H_L(t) &= \frac{\hbar}{2}\begin{pmatrix} \omega_0 & 2\Omega_{\mathrm{R}}(t)\cos(\omega_D(t)t+\varphi) \\ 2\Omega_{\mathrm{R}}(t)\cos(\omega_D(t)t+\varphi) & -\omega_0 \end{pmatrix} \\ &= \frac{\hbar}{2}\begin{pmatrix} \omega_0 & \Omega_{\mathrm{R}}(t)(e^{i(\omega_D(t)t+\varphi)}+e^{-i(\omega_D(t)t+\varphi)}) \\ \Omega_{\mathrm{R}}(t)(e^{i(\omega_D(t)t+\varphi)}+e^{-i(\omega_D(t)t+\varphi)}) & -\omega_0 \end{pmatrix}. \end{aligned} \tag{1}$$

The transformation $H_0 = UH_LU^\dagger + i\hbar\frac{\partial U}{\partial t}U^\dagger$ brings us into a reference frame rotating with the driving field frequency. Here, U is the unitary matrix $U(t) = e^{i/\hbar H_D(t)t}$ defined by the applied driving field frequency:

$$H_D(t) = \frac{\hbar}{2}\begin{pmatrix} \omega_D(t) & 0 \\ 0 & -\omega_D(t) \end{pmatrix}. \tag{2}$$

Note, that this transformation changes the description from the laboratory frame $H_L(t)$, a frame of constant rotation rate, to the rotating frame of the driving field $H_0(t)$ rotating at a non-constant rate. This is a non-standard case of transformation leading to the appearance of time-dependent terms on the diagonal of $H_0(t)$. Explicitly, the time dependence of $\omega_D(t)$ causes the second term of the transformation $\left(i\hbar\frac{\partial U}{\partial t}U^\dagger\right)$ to contain two components ($-\hbar/2\cdot\omega_D(t)$ and $-t\hbar/2\cdot\partial\omega_D(t)/\partial t$), which is in stark contrast to driving fields of fixed frequency. Explicitly, for the Hamiltonian in the driving field frame (rotating at a time-varying rate) one obtains

$$\begin{aligned} H_0(t) &= \frac{\hbar}{2}\begin{pmatrix} \Delta(t)+\dot{\Delta}(t)t & \Omega_{\mathrm{R}}(t)e^{i\omega_D(t)t}(e^{-i(\omega_D(t)t+\varphi)}+e^{-i(\omega_D(t)t+\varphi)}) \\ \Omega_{\mathrm{R}}(t)e^{-i\omega_D(t)t}(e^{i(\omega_D(t)t+\varphi)}+e^{-i(\omega_D(t)t+\varphi)}) & -(\Delta(t)+\dot{\Delta}(t)t) \end{pmatrix} \\ &= \frac{\hbar}{2}\begin{pmatrix} \Delta(t)+\dot{\Delta}(t)t & \Omega_{\mathrm{R}}(t)e^{-i\varphi} \\ \Omega_{\mathrm{R}}(t)e^{i\varphi} & -(\Delta(t)+\dot{\Delta}(t)t) \end{pmatrix}. \end{aligned} \tag{3}$$

where we rewrite the driving field detuning as $\Delta(t) = \omega_0 - \omega_D(t)$ and its temporal derivative $\dot{\Delta}(t) = -\dot{\omega}_D(t)$. In this derivation we performed the rotating wave approximation to average out fast oscillating frequency components.

2 Driving field parameters

To ensure working in the experimentally accessible regime the free parameters were set to $\Omega_0 = 3.5\,\mathrm{MHz}$, $\Delta_0 = 1\,\mathrm{MHz}$ and $\tau = 2\pi \times 0.8/(2\Omega_0)$ for our system limited by $\Omega_{\max} \approx 7.5\,\mathrm{MHz}$. For completeness, find the expressions for the driving field parameters utilized to realize the superadiabatic geometric Pauli-X gate below.

$$\Omega_{\mathrm{R}}(t) = \begin{cases} \Omega_0 \left[1 + \cos\frac{\pi t}{\tau}\right], & 0 \le t < \tau \\ \Omega_0 \left[1 - \cos\frac{\pi(t-\tau)}{\tau}\right], & \tau \le t < 2\tau \\ \Omega_0 \left[1 + \cos\frac{\pi(t-2\tau)}{\tau}\right], & 2\tau \le t < 3\tau \\ \Omega_0 \left[1 - \cos\frac{\pi(t-3\tau)}{\tau}\right], & 3\tau \le t \le 4\tau \end{cases} \tag{4}$$

and

$$\Delta_{\mathrm{S}}(t) = \begin{cases} \Delta_0 \left[\cos\frac{\pi t}{\tau} - 1\right], & 0 \le t < \tau \\ \Delta_0 \left[\cos\frac{\pi(t-\tau)}{\tau} + 1\right], & \tau \le t < 2\tau \\ \Delta_0 \left[\cos\frac{\pi(t-2\tau)}{\tau} - 1\right], & 2\tau \le t < 3\tau \\ \Delta_0 \left[\cos\frac{\pi(t-3\tau)}{\tau} + 1\right], & 3\tau \le t \le 4\tau \end{cases} \tag{5}$$

and

$$\varphi + \phi_s(t) = \begin{cases} \phi_s(t) + \widetilde{\varphi}_1', & 0 \le t < \tau \\ \phi_s(t) + \widetilde{\varphi}_2', & \tau \le t < 3\tau \\ \phi_s(t) + \widetilde{\varphi}_1', & 3\tau \le t \le 4\tau \end{cases}. \tag{6}$$

As for the Pauli-Z gate the acquired geometric phase γ' can be chosen via the relation $\gamma' = \pi - (\widetilde{\varphi}_2' - \widetilde{\varphi}_1')$.

In supplementary Supp.Fig.1 the driving field parameter of the superadiabatic geometric Pauli-X and Pauli-Z gate used for the experimental realization are presented. Note, while the Rabi-frequency $\Omega_{\mathrm{S}}(t)$ and phase $\varphi + \phi_s(t)$ of the Pauli-X and Pauli-Z gate are identical except for a time shift of τ, the driving field detuning functions $\Delta(t)$ defer strongly and the maximal absolute detuning of the Pauli-Z gate is twice as high as the one of the Pauli-X gate. This difference is originating from the obtained solution $\Delta(t)$ of the differential equation $\Delta(t) + \dot{\Delta}(t)t = \Delta_{\mathrm{S}}(t)$. From the mathematical point of view the effective superadiabatic detuning $\Delta_{\mathrm{S}}(t)$ are again identical up to a time shift of τ. However, involved with the different amplitudes of the detunings $\Delta(t)$ there might be some experimental implications for realizations choosing large Δ_0.

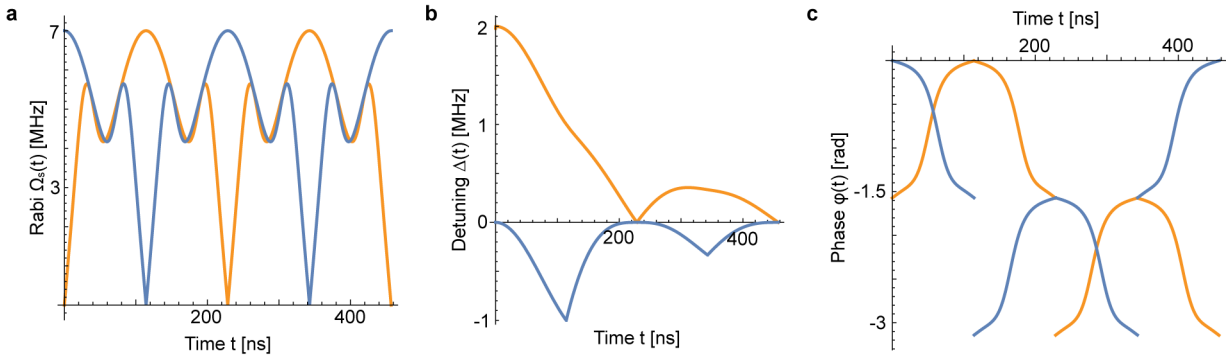

Supplementary Figure 1. Driving field parameters as a function of time. (a) Shows the applied Rabi frequency $\Omega_{\mathrm{R}}(t)$ of the superadiabatic geometric quantum gate, (b) the driving field detuning $\Delta(t)$ (not to be confused with $\Delta_{\mathrm{S}}(t)$) and (c) the phase $\varphi + \phi_s(t)$ for Pauli-X (blue) and Pauli-Z (orange) gate, respectively

3 Standard Quantum Process Tomography

The standard quantum process tomography employed in this work is a modified version of the one presented in Ref.[1], which was designed for the reconstruction of the process matrix of evolutions in the three-dimensional Hilbert space $\mathscr{H}^3$. Switching to two-dimensional $\mathscr{H}^2$ Hilbert space in the case of our super-adiabatic geometric realizations requires the choice of an appropriate set of basis operators. We chose the Pauli matrices $\boldsymbol{\sigma}$ complemented by the identity matrix (see Supp.Tab.1). The pulse sequences generating the basis states are illustrated in Supp. Tab.2.

Supplementary Table 1. Convention of the basis operators used in the quantum process tomography for the gates performed on the two dimensional Hilbert space $\mathscr{H}^2$.

E_m	Pauli Operator	explicit expression	matrix representation
E_1	σ_0	$\|0\rangle\langle 0\| + \|-\rangle\langle -\|$	$\begin{pmatrix} 1 & 0 \\ 0 & 1 \end{pmatrix}$
E_2	σ_x	$\|0\rangle\langle -\| + \|-\rangle\langle 0\|$	$\begin{pmatrix} 0 & 1 \\ 1 & 0 \end{pmatrix}$
E_3	σ_y	$i\|0\rangle\langle -\| - i\|-\rangle\langle 0\|$	$\begin{pmatrix} 0 & -i \\ i & 0 \end{pmatrix}$
E_4	σ_z	$\|0\rangle\langle 0\| - \|-\rangle\langle -\|$	$\begin{pmatrix} 1 & 0 \\ 0 & -1 \end{pmatrix}$

Supplementary Table 2. Pulse sequence for quantum process tomography. EXC represent an initialization into the $m_s = 0$ state by a laser pulse. $(\tau)_j$ symbolizes a microwave j-pulse of length τ. DET means the readout out of the $m_s = 0$ population by excitation for 300 ns and simultaneous fluorescence detection.

Ψ_j	explicit expression	initialization	readout
Ψ_1	$\|0\rangle$	EXC	DET
Ψ_2	$\|-\rangle$	$\mathrm{EXC} + (\pi)_{\bar{y}}$	$(\pi)_y + \mathrm{DET}$
Ψ_3	$\frac{1}{\sqrt{2}}(\|0\rangle + \|-\rangle)$	$\mathrm{EXC} + \left(\frac{\pi}{2}\right)_{\bar{y}}$	$\left(\frac{\pi}{2}\right)_y + \mathrm{DET}$
Ψ_4	$\frac{1}{\sqrt{2}}(\|0\rangle + i\|-\rangle)$	$\mathrm{EXC} + \left(\frac{\pi}{2}\right)_{\bar{x}}$	$\left(\frac{\pi}{2}\right)_x + \mathrm{DET}$

4 Randomized benchmarking

The randomized benchmarking analysis is performed following the approach of Knill *et al.*[2]. In essence, randomly generated sequences of gate operations of different length are utilized to measure the discrepancy between the expected and experimentally obtained result as a function of the sequence length. In order to observe the error scaling independently of the applied sequence the errors are randomized by means of randomly chosen Pauli pulses which are interleaved with the $\pi/2$-rotations assumed to perform the computation. The combination of one Pauli randomization pulse with one $\pi/2$-rotation is typically referred to as computational gate. By additionally varying the sequence itself, an additional averaging is obtained. The increase of the error probability with the number of computational gates l leads to a decay of the average fidelity. The experimental randomized benchmarking data were fitted by the function $f(l) = 1 - ((1-\alpha_n\varepsilon_m)(1-\alpha_n\varepsilon_g)^l + 1)/\alpha_n$, where $\alpha_n = 2^n/(2^n-1)$ is a factor depending on the number of qubits n involved[3]. The error probability ε_m accounts for errors in the state preparation, the final projection Pauli randomization pulse combination and the readout.

The sequence generation is performed as follows: $N_G = 4$ random sequences $\mathscr{G} = \{G_1, \dots\}$ of $\pi/2$-rotations around the x, z, $\bar{x}$, and $\bar{z}$-axis are cropped to $N_l = 13$ different lengths $l_k = \{2,4,6,8,10,14,18,22,26,30,34,40,48\}$. For each sequence the final state is calculated and a randomly chosen projective pulse R added under the condition that the output state at the end of the sequence is one of the system eigenstates. Each individual sequence is then Pauli randomized $N_P = 8$ times by randomly choosing a sequence $\mathscr{P} = \{P_1, \dots\}$ (consisting out of π-rotations around x, z, y, $\bar{x}$, $\bar{y}$, and $\bar{z}$-axis as well as the identity operation $\gamma = 0, \pi$) of length $l_k + 2$. Subsequently, the total sequence $\mathscr{S} = P_{l_k+2} R P_{l_k+1} G_{l_k} \dots G_1 P_1$ is generated. By comparing the measured output state with the expected one the average gate fidelity is obtained. The average gate fidelity is calculated as the mean over the $N = N_P \cdot N_G = 32$ measurements for each gate length l_k. Uncertainties are estimated by the standard error of the mean $\sigma_{\text{mean}} = \sigma/\sqrt{N}$. All operations in $\mathscr{S}$ are performed by SAGQGs.

Randomized benchmarking of the dynamic gate set follows equivalently when replacing the SAGQGs by dynamic π and $\pi/2$-pulses. The gates performing the computation are assumed to be $\pi/2$-rotations around x, y, $\bar{x}$, and $\bar{y}$-axis. Rotations around the z-axis during the Pauli randomization are realized by appropriately adjusting the phase of the driving field. Identity operations are performed by rotations of 2π around x and $\bar{x}$.

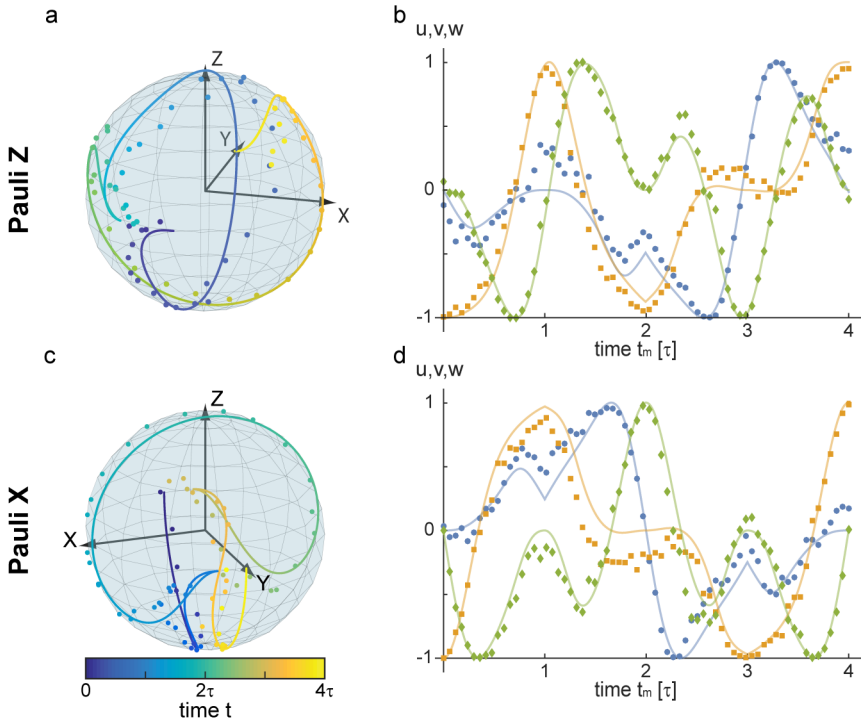

Supplementary Figure 2. Bloch sphere trajectories of the Pauli-Z (a,b) and Pauli-X (c,d) gate operation acting on the initial states $|\psi_i\rangle = 1/\sqrt{2}(|1\rangle - i|0\rangle)$, respectively. Bloch vector components are given by $u(t) = \rho_{10}(t) + \rho_{01}(t)$ (blue), $v(t) = i(\rho_{01}(t) - \rho_{10}(t))$ (orange) and $w(t) = \rho_{00}(t) - \rho_{11}(t)$ (green), where $\rho(t)$ is the density matrix representationof the instantaneous state.

5 Bloch sphere trajectory

In Supp.Fig.2 the Bloch sphere trajectory for Pauli-Z (a,b) and Pauli-X (c,d) gates acting on the initial states $|\psi_i\rangle = \frac{1}{\sqrt{2}}(|1\rangle - i|0\rangle)$ are presented. Analogue measurements of the Bloch sphere trajectory for the initial state $|\psi_i\rangle = \frac{1}{\sqrt{2}}(|1\rangle + |0\rangle)$ are shown in Supp.Fig.3. For the Pauli-X gate the Bloch sphere trajectory follows the "orange slice"-like trajectory, since the initial state $|\psi_i\rangle$ corresponds to one of the energy eigenvalue $|\lambda_{\pm}(0)\rangle$ of the Hamiltonian at time $t = 0$.

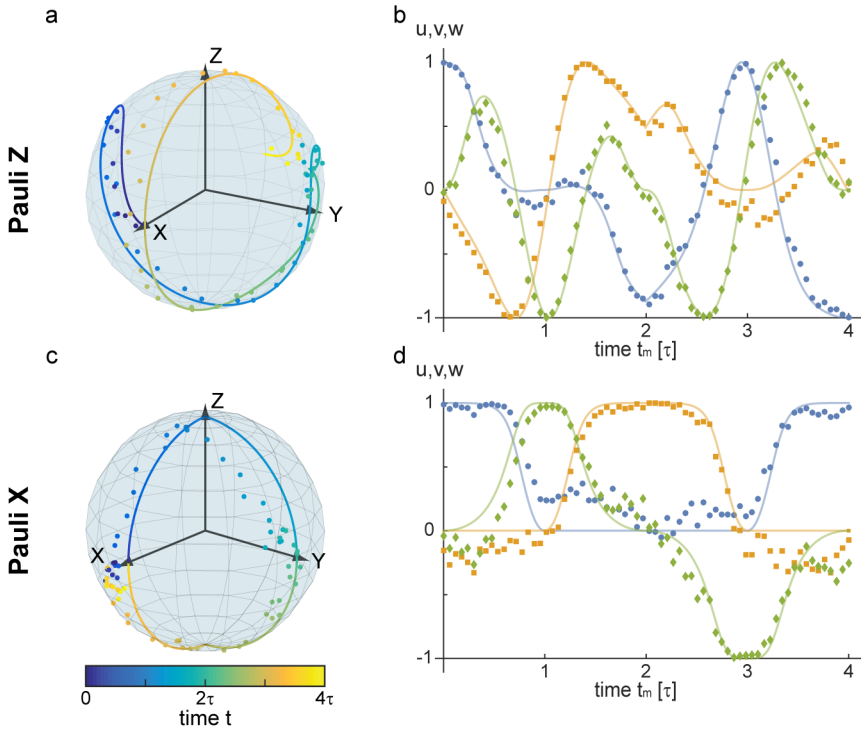

Supplementary Figure 3. Bloch sphere trajectories of the Pauli-Z (a,b) and Pauli-X (c,d) gate operation acting on the initial states $|\psi_i\rangle = 1/\sqrt{2}(|1\rangle + |0\rangle)$, respectively. Bloch vector components are given by $u(t) = \rho_{10}(t) + \rho_{01}(t)$ (blue), $v(t) = i(\rho_{01}(t) - \rho_{10}(t))$ (orange) and $w(t) = \rho_{00}(t) - \rho_{11}(t)$ (green), where $\rho(t)$ is the density matrix representation of the instantaneous state.

References

1. Arroyo-Camejo, S., Lazariev, A., Hell, S. W. & Balasubramanian, G. Supplementary information: Room temperature high-fidelity holonomic single-qubit gate on a solid state spin. *Nat. Commun.* **5** (2014). URL http://dx.doi.org/10.1038/ncomms5870. DOI 10.1038/ncomms5870.

2. Knill, E. *et al.* Randomized benchmarking of quantum gates. *Phys. Rev. A* **77** (2008). URL http://dx.doi.org/10.1103/PhysRevA.77.012307. DOI 10.1103/PhysRevA.77.012307.

3. Gaebler, J. *et al.* Randomized bbenchmarking of multiple gates. *Phys. Rev. Lett.* **108** (2012). URL http://dx.doi.org/10.1103/PhysRevLett.108.260503. DOI 10.1103/PhysRevLett.108.260503.